Control of polarized iodine atom branching ratio in NaI photodissociation

Babak H. Hosseini,[1,2,*] H. R. Sadeghpour,[1] and N. Balakrishnan[3]

[1]*ITAMP, Harvard-Smithsonian Center for Astrophysics, Cambridge, Massachusetts 02138, USA*
[2]*Fakultät für Physik und Astronomie, Universität Heidelberg, Heidelberg, Germany*
[3]*Department of Chemistry, University of Nevada Las Vegas, Las Vegas, Nevada 89154, USA*
(Received 5 August 2004; published 2 February 2005)

We report branching ratios between the ground and excited states of iodine atoms in the photodissociation of sodium iodide. We employ wave packet propagation techniques to study the optimal production of polarized iodine atoms and find experimentally realizable laser parameters to control the outcome. Application of a learning algorithm shows that the product branching can be controlled by suitably varying the time delay, the chirp, and the relative phase of the pump and control laser pulses. Periodic modulation of the polarized iodine atom branching ratio as a function of the delay between the firing of the two ultrashort laser pulses provides interesting insights into the photodissociation process.

I. INTRODUCTION

Active control and manipulation of atomic and molecular transitions have been at the forefront of research in physics over the last couple of decades. The invention of stable ultrashort laser pulses and techniques for laser cooling and magnetic trapping of atoms has led to major discoveries in science: the macroscopically coherent atomic and molecular matter and the Bose-Einstein condensate [1–3], and real-time processing of biological macromolecules being a few examples. The nearly still motion of atoms in a Bose-Einstein condensate provides unprecedented opportunities for performing ultrahigh-resolution spectroscopy of atoms and molecules [4], while the stability of ultrashort laser pulses [5–9] enables real-time viewing of the intricate processes within a complex molecule. In the realm of molecular spectroscopy, quantum control of transitions is now routinely possible and optimized techniques for achieving the desired outcome are available.

Diatomic molecules have been prototypes for the study of quantum control in both time and frequency domains [10–14]. Sodium iodide (NaI) is a classical example of such a diatomic molecule and femtosecond pump-probe studies of this system by Zewail and co-workers [15–20] have provided considerable insights into the dissociation dynamics. For sodium iodide, all available calculations of quantum control have treated the molecule as a two-level system [21–31] with the lowest excited $2\,^{1}\Sigma^{+}$ covalent potential curve and the bound ionic $X\,^{1}\Sigma^{+}$ potential curve crossing at an internuclear separation of about $13a_0$. This is a typical scenario with alkali-metal halides [32] and the crossing arises because the energy required to dissociate the molecules into ions is larger than that required to separate them into neutral atoms. However, an accurate treatment of the photodissociation dynamics of NaI should include both the ground and excited spin-orbit states of the iodine atom as neutral dissociation channels as well as the ion-pair formation channel.

Recently, *ab initio* potential energy curves, spin-orbit coupling matrices, and transition and permanent dipole matrix elements for the low-lying electronic states of NaI have been computed and photodissociation dynamics of NaI employing these potential curves has been reported [33]. It was found that the substantial energy difference (0.942 eV) between the ground I($^{2}P_{3/2}$) and the excited I($^{2}P_{1/2}$) atoms quantitatively changes the behavior of the potential curves near the crossing region. In particular, the inclusion of spin-orbit coupling led to a second crossing between the ionic curve and covalent curve separating to the Na+I($^{2}P_{1/2}$) fragments at an internuclear separation of $23.7a_0$.

In this paper, we report time-dependent wave packet calculations of the photodissociation process with the aim of controlling the branching ratio between the ground $(^{2}P_{3/2})$ and the first excited $(^{2}P_{1/2})$ states of the iodine atom and the I$^{-}(^{1}S)$ and Na$^{+}(^{2}P)$ ion pairs. We use previously reported [33] diabatic potential energy curves and coupling matrix elements and investigate the wave packet evolution on three coupled potential energy curves in the presence of two ultrashort laser pulses—a pump and a control pulse. This approach bears resemblance to the Rice-Tannor control scheme in which an initial pump pulse transfers amplitude from the ground state to an excited state and a second pump pulse transfers amplitude in the opposite direction, and thereby modifies the branching ratio between the two product channels [14]. We use a learning algorithm to optimize a subset of laser parameters and obtain optimal pulses to control the branching ratio.

By tuning the laser parameters, the learning algorithm calculates the best experimentally realizable scenarios for controlling the production of polarized iodine atoms. Additionally, we find modulation of the branching ratio as a function of the time delay with a characteristic period of about one picosecond. We show that photodissociation of NaI could be a useful source of polarized iodine atoms. In a recent study, it has been shown that the production of polarized atoms in photodissociation leads to distinct angular momentum distributions of ground state and excited state cofragments [34].
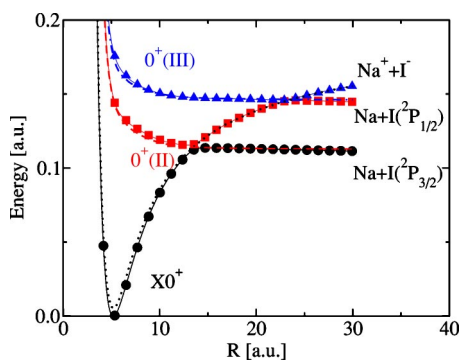
*Electronic address: bhadjiho@cfa.harvard.edu

FIG. 1. Adiabatic and diabatic potentials obtained by including spin-orbit coupling. The adiabatic potential curves are denoted by symbols and solid lines: $X0^+$ (circles); $A0^+$ (squares); $B0^+$ (triangles). The corresponding diabatic potential curves are denoted by the broken lines: ionic (dotted curve); ground covalent state (dashed curve); excited covalent state (dash-dotted curve).

II. THEORETICAL FRAMEWORK

A. Electronic potentials

The potential curves relevant to the present study are the $\Omega=0^+$ adiabatic potential curves, where $\Omega=|\Lambda+\Sigma|$, and Λ and Σ are, respectively, the components of the total orbital and spin angular momenta of the electrons along the internuclear axis. The three lowest $\Omega=0^+$ states are the ground ionic state $X0^+$ and the two covalent states $A0^+$ and $B0^+$ which dissociate, respectively, to the $Na+I(^2P_{3/2})$ and $Na+I(^2P_{1/2})$ atomic limits. The ionic state $X0^+$ breaks up into $Na^+(^2P)$ and $I^-(^1S)$ ions. The 0^+ potential curves are shown in Fig. 1. It is seen that the asymptotic spin-orbit splitting of $I(^2P_{3/2})$ and $I(^2P_{1/2})$ atoms is correctly reproduced by the *ab initio* calculations. More details of the *ab initio* potentials, including radial dependence of the dipole and spin-orbit coupling matrix elements, are given in our earlier work [33].

In the present study, we use the diabatic representation in which the kinetic energy operator for the nuclear motion is diagonal. In this representation, the couplings are restricted to the off-diagonal elements of the potential energy matrix and it is more convenient for numerical calculations. The details of the adiabatic to diabatic transformation are discussed in Ref. [33].

B. Wave packet propagation

The Schrödinger equation in the diabatic representation for the three-channel problem can be written as

$$i\hbar\frac{\partial\mathbf{\Psi}(R,t)}{\partial t}=\mathbf{H}^d\mathbf{\Psi}(R,t)=\left[-\frac{\hbar^2}{2\mu}\mathbf{I}\frac{d^2}{dR^2}+\mathbf{V}^d\right]\mathbf{\Psi}(R,t) \quad (1)$$

where $\mu=35\,357$ a.u. is the reduced mass of the molecule, $\mathbf{I}$ is the 3×3 unity matrix, and $\mathbf{\Psi}$ is a three-component vector, each component representing the part of the wave function on the electronic states $X0^+$, $A0^+$, and $B0^+$. It should be emphasized that in the diabatic representation the potential matrix $\mathbf{V}^d$ is nondiagonal and carries the nonadiabatic couplings as off-diagonal elements. The coupled-channel equations are

solved using the split-operator method [35,36] which employs a symmetric splitting of the kinetic and potential energy operators. We have previously applied this approach to compute photoabsorption spectra of LiF [32], NaI [33], and HI [37]. For LiF we have demonstrated the accuracy by comparing with results obtained from time-independent quantum calculations while for NaI excellent agreement was obtained with experimentally derived pump-probe signals. For the photodissociation of HI [37], quantitative agreement was obtained with measured values of photoabsorption cross sections.

In the diabatic representation, the wave packets are initialized as

$$\psi_1(R,t=0)=\phi_{v''j''}(R),$$

$$\psi_2(R,t=0)=0,$$

$$\psi_3(R,t=0)=0, \quad (2)$$

where $\phi_{v''j''}(R)$ is a rovibrational eigenfunction of the ionic potential corresponding to vibrational and rotational quantum numbers v'' and j''. A grid of 2048 points with $3.0a_0 \leq R \leq 50.0a_0$ is used to represent the wave functions on the three potential curves.

The probability flux in each channel i is given by

$$J_i(t)=\frac{\hbar}{\mu}\text{Im}\left[\psi_i(R,t)\frac{\partial\psi_i(R,t)}{\partial R}\right]_{R=R_f} \quad (3)$$

where $i\in\{1,2,3\}$ corresponds to Na^++I^-, $Na+I(^2P_{3/2})$, and $Na+I(^2P_{1/2})$ products, respectively, and R_f is the location of the flux calculation. An absorbing potential is placed at internuclear separations $R\geq45.0a_0$ to avoid wave packet reflection from the grid boundaries. The probability in each dissociative channel is obtained by integrating the corresponding flux over the time interval $[0,T]$ in which it is recorded. For example, the probabilities to find ground and excited state iodine atoms are given by

$$p(I)=p=\int_0^T J_2(t)dt, \quad (4a)$$

$$p(I^*)=p^*=\int_0^T J_3(t)dt. \quad (4b)$$

We use a two-pulse scheme to control the branching ratio for the production of excited vs ground state iodine atoms, p^*/p, or simply I^*/I. The two Gaussian-shaped laser pulses, the first being the pump and the second the control pulse, are given by

$$E_1(t)=\hat{E}_1\exp\left(-\frac{1}{2}\left[\frac{(t-t_1)}{\tau_1}\right]^2\right)\cos(\omega_1 t),$$

$$E_2(t) = \hat{E}_2 \exp\left(-\frac{1}{2}\left[\frac{(t-t_2)}{\tau_2}\right]^2\right)\cos[\omega_2 t + \alpha_2(t-t_2)^2 + \phi],$$

$$(5)$$

where α_2 is a linear chirp for the second laser, and ϕ is the relative phase between the two laser pulses. Chirped pulses have varying central frequency and longer duration compared to unchirped pulses. In the presence of the laser pulses, the full diabatic Hamiltonian takes the form

$$\mathbf{H}_{full}^d(t)$$
$$= \begin{Bmatrix} H_{11}^d - D_{11}^d(R)E_1(t) & H_{12}^d & H_{13}^d \\ H_{21}^d & H_{22}^d & H_{23}^d - D_{23}E_2(t) \\ H_{31}^d & H_{32}^d - D_{23}E_2(t) & H_{33}^d \end{Bmatrix}.$$

$$(6)$$

In the above expression, $D_{11}^d(R)$ is the strongly R-dependent dipole matrix element for optical transitions in the diabatic ionic $X0^+$ channel, and we have taken the transition dipole matrix element D_{23} to be weakly dependent on the internuclear separation and equal to unity. The pump-control scheme can be used effectively to control the branching ratio I^*/I if certain parameters of the pulses are suitably chosen. The implementation of a genetic algorithm yields optimal pulses from a subset of laser parameters which minimize or maximize the production of excited iodine.

C. Genetic algorithm

The learning algorithm we use is a so-called genetic algorithm (GA). Genetic algorithms are inspired by selection mechanisms which occur in nature [38,39]. A genetic algorithm is an iterative procedure that maintains a population of candidate solutions, which are also called structures, to the objective or fitness function $f(\mathbf{x})$. The procedure employs stochastics to guide a highly exploitative search. In our case, $f(\mathbf{x}) = I^*/I$ is the branching ratio between the excited and the ground state iodine atoms, and $\mathbf{x} = (t_d, \phi, \alpha_2)$ is a triplet containing a subset of laser parameters which are subject to optimization. The parameter $t_d = t_2 - t_1$ is the time delay between the firings of the two laser pulses with relative phase ϕ, and α_2 is a linear chirp factor for the second laser—all other pulse parameters in Eq. (5) are fixed. We keep the intensities low at $\hat{E}_1 = \hat{E}_2 = 2.57$ GV/m to avoid multiphoton effects; the first laser is fired at $t_1 = 150$ fs and the width of the pulses are fixed at $\tau_1 = \tau_2 = 50$ fs. The set of all possible triplets $\mathbf{x}$ defines the parameter space Γ. The GA encodes the triplets $\mathbf{x}$ internally into a string, which can be, e.g., a sequence of 0's and 1's or simply a real number. It explores the parameter space Γ using the wave packet calculation described above. The GA starts out with a random population of different laser parameters sets

$$P_0 = (\mathbf{x}_1, \mathbf{x}_2, \ldots, \mathbf{x}_n),$$

$$(7)$$

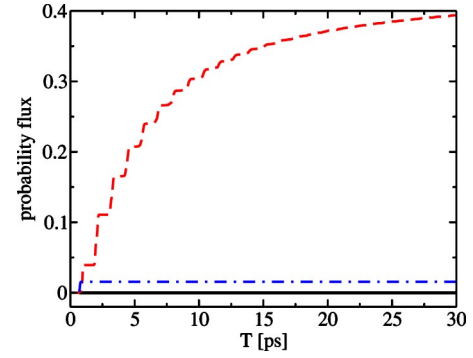and runs the wave packet calculation with these parameters to obtain a fitness value for each pulse,

FIG. 2. Dissociation probability vs time: probability flux J_2 (dashed line), corresponding to the production of I($^2P_{3/2}$); probability flux J_3 (dash-dotted line), corresponding to the production of I($^2P_{1/2}$). The ion-pair formation (solid line) is nearly zero.

$$f(P_0) = (f(\mathbf{x}_1), f(\mathbf{x}_2), \ldots, f(\mathbf{x}_n)).$$

$$(8)$$

In the next step, a new population is formed based on the outcome of Eq. (8). Three operators are applied to create a new generation

$$P_{i+1} = (\mathbf{M} \circ \mathbf{C} \circ \mathbf{R})P_i$$

$$(9)$$

where $\mathbf{R}$, $\mathbf{C}$, and $\mathbf{M}$ are, respectively, the reproduction, the crossover, and the mutation operators. The reproduction operator will randomly copy the individual elements in P_i weighing them only according to their fitness function value $f(\mathbf{x})$ obtained in Eq. (8), which means that structures with higher fitness are more likely to be copied into the new set. Through the next step, crossover, variations are introduced into the new generation in order to explore other points in the parameter space Γ than already present in the current population. Our crossover rate was set to 0.6, which meant that about 60% of the encoded information in the string was interchanged between the members of the population to create a new generation. The last operator, mutation, plays a secondary role in simple GAs. It introduces new search points in Γ at random, but at a small rate.

The genetic algorithm code we employed to optimize the subset of laser parameters is freely available [40]. We modified the algorithm so as to be able to run in a multiprocessor environment. A wave packet propagation time of $T \approx 17$ ps translates into approximately 1.5 h computation time for each trial, i.e., an evaluation of a structure.

III. RESULTS AND DISCUSSION

We tuned the first laser at a wavelength of $\lambda = 320$ nm, which is right at the maximum of the partial photoabsorption cross section of the ground covalent ($^2P_{3/2}$) state. This amounts to transferring amplitude from the ionic ground state to the covalent one and leads to the production of iodine atoms in the ground state. In Fig. 2, we show the integrated probability flux on the lower and upper excited states as a function of integration time. In these calculations only the first laser is turned on. It is seen that the dominant product is
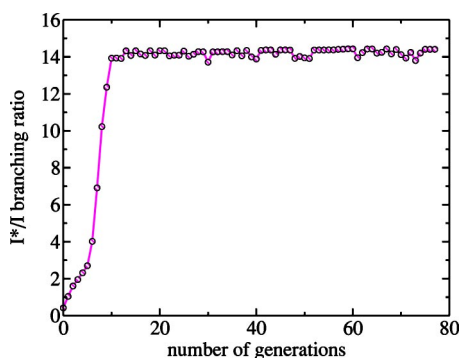
FIG. 3. The ratio of excited to ground state iodine atoms (fitness function) as a function of the number of generations in the genetic algorithm.

the ground state iodine atom and that the fitness function $f(\mathbf{x})=[\text{I}^*/\text{I}]$ is very small, $\text{I}^*/\text{I}\approx 0.043$ after a propagation time of $T=17$ ps.

It is possible to change the branching ratio quite substantially by switching on the second laser pulse with suitably chosen parameters. This is facilitated by the GA which maximizes the fitness function $f(\mathbf{x})$ and yields significantly more iodine atoms in the excited state than the ground state. The results are shown in Fig. 3. Approximately 80 generations were evaluated with a size of $n=50$ structures in each one. After only 20 generation cycles, the GA converges to a very stable value for $f(\mathbf{x})$ and therefore has found a subspace in the parameter space favoring high values of I^*/I.

In Figs. 4(a)–4(c) we show the distribution of time delay, chirp, and phase values of the 50 fittest structures resulting from the GA. Most of the time delay values bunch up at short times and also at around $1.1-1.3$ ps. For the laser chirp only two values, $\pm 3.2\times 10^{-6}$ s^{-2}, are found while a broader distribution is obtained for ϕ with a slight preference for $\phi < 0.8\pi$. These distributions lead to an important question: what can we actually learn about the physics of the system from the application of the learning algorithm? To see the significance of the distributions, we took the best pulse resulting from the GA, $\mathbf{x}^*=(t_d^*,\alpha_2^*,\phi^*)=(118 \text{ fs},-3.2 \times 10^{-6} \text{ s}^{-2},4/15\pi)$ and sliced the parameter space from this point off along the axes.

In Fig. 5 we show the I^*/I branching ratio as a function of the time delay t_d. It exhibits a pronounced periodic behavior with peaks separated by $1.1-1.3$ ps coinciding with the period of oscillation of the wave packet on the $A0^+$ state [33]. As shown in Fig. 2 the excited state product is formed in the first passage of the wave packet through the second crossing in approximately 800 fs. On the other hand, the ground state product probability shows a stepwise buildup (see Fig. 2) through bursts in the probability flux $J_1(t)$, separated by about 1.3 ps—the vibrational period of the wave packet on the $A0^+$ potential [33]. The recurring peaks in the branching ratio as a function of the time delay between the pump and control laser pulses are due to the dispersion of the wave packet in the ground ionic and $A0^+$ covalent states and the nonadiabatic coupling between these two electronic states. Even though the wave packet was initially prepared in the ground ionic state, amplitude is constantly transferred to the
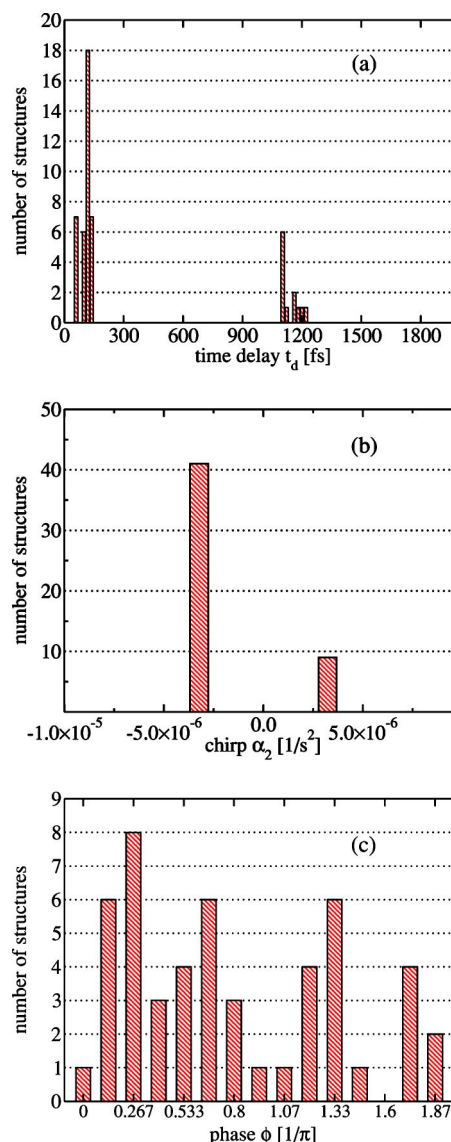

FIG. 4. Distributions of the time delay (t_d), chirp phase (α_2), and phase (ϕ) of the 50 best structures obtained by the GA.

ground and excited covalent states through the nonadiabatic couplings. The second laser transfers amplitude between the two covalent states. When the time between the firings of the two laser pulses commensurate with the time required for the wave packet to make a round trip in the $A0^+$ covalent potential curve, the branching ratio of the excited to ground iodine atoms maximizes and population is efficiently transferred from the ground covalent state to the excited covalent state, thus contributing to a peak in Fig. 5.

The dispersion of the wave packet is illustrated in Figs. 6(a)–6(d), where we show snapshots of the time evolution of the wave packets on the diabatic curves with the second laser turned off. For $t\leq 300$ fs, the ground state wave packet is excited by the first laser on the $X0^+$ curve. Almost instantly, this excited wave packet is distributed onto the $A0^+$ and $B0^+$ covalent curves due to the diabatic couplings [Fig. 6(a)]. As the wave packets move outward and approach the crossings, parts of them are transferred to the ionic curve [Fig. 6(b)]. The remaining parts dissociate after passing the region of the
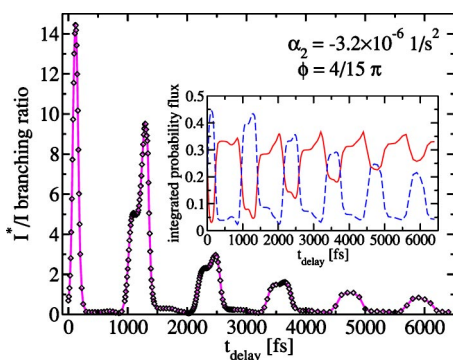
FIG. 5. I^*/I branching ratio as a function of the time delay with all other parameters fixed. The best pulse $\mathbf{x}^*$ serves as the origin. Inset: I and I^* dissociation probabilities as functions of the time delay: ground $I(^3P_{3/2})$ channel (solid line) and excited $I(^3P_{1/2})$ channel (dashed line).

crossings between the ionic and covalent curves yielding $I(^2P_{3/2})$ and $I(^2P_{1/2})$ atoms. Because of the flat shape of the $B0^+$ potential near its crossing with the ionic curve and the small values of the diabatic couplings between the two potentials in the vicinity of the crossing, almost all of the wave packet on the $B0^+$ potential undergoes direct dissociation yielding iodine atoms in the excited state. This explains why the I^* product is formed in a single burst. Large parts of the $A0^+$ wave packet, however, are transferred back to the ionic channel on the way out [Fig. 6(b)]. This part is then reflected on the outer turning point of the $X0^+$ curve and on its way inward is again transferred onto the $A0^+$ potential [Fig. 6(c)], starting a new cycle of wave packet motion [Fig. 6(d)]. This oscillatory transfer of amplitude between the ionic $X0^+$ and the covalent $A0^+$ curve explains the leaking of the $I(^2P_{3/2})$ wave packet with a period of about 1.3 ps and hence the stepwise buildup of the dissociation probability (Fig. 2). This periodic exchange of amplitude and the ensuing dynamics is also reflected in the results of the GA. Every time the ionic wave packet is transferred to the $A0^+$ potential on its inward motion, the second laser will take it to the excited covalent channel, thus increasing the yield of I^* atoms. In this sense, the second laser is probing amplitude in the $A0^+$ channel. (Animations illustrating these oscillations can be found here [41].)
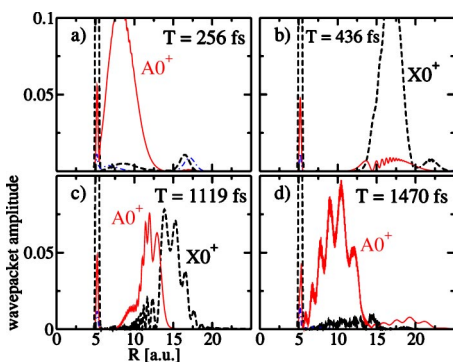

FIG. 6. Snapshots of the wave packets on the three diabatic curves at different time intervals: ground ionic (dashed line); ground covalent (solid line); and excited covalent (dash-dotted line).
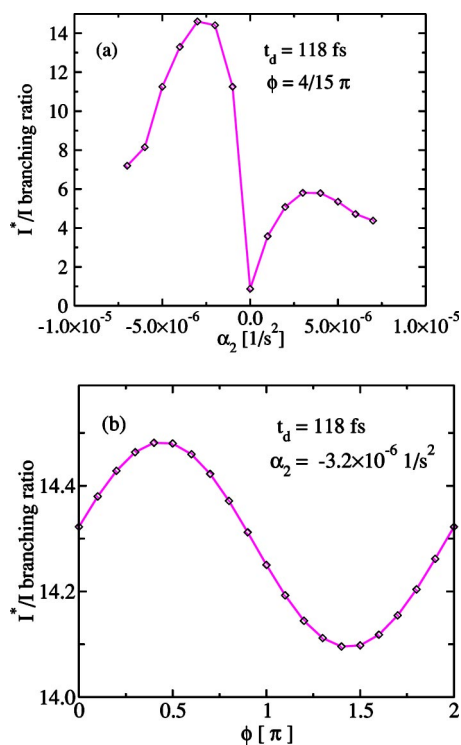

FIG. 7. I^*/I branching ratio as a function of the laser chirp (a) and the relative phase (b) with all other parameters fixed. The best pulse $\mathbf{x}^*$ serves as the origin.

The periodic peaks in the time-delay spectrum (Fig. 5) show shoulders to the left of the maxima in the branching ratio. These shoulders are due to the difference in the wave packet oscillation periods in the $X0^+$ and $A0^+$ curves. The part of the ionic wave packet which has not leaked to the covalent channel gets reflected from the inner turning point about 200 fs prior to the covalent wave packet on the $A0^+$ potential. As the ionic wave packet traverses the crossing, part of it is transferred to the $A0^+$ curve, just ahead of the arrival of the slower-moving $A0^+$ covalent wave packet. Thus, for a brief period of time, there is a buildup of amplitude on the $A0^+$ potential. The second laser transfers this amplitude onto the $B0^+$ potential which yields I^* and hence the peaks to the right of the shoulder peaks in Fig. 5. The peak amplitudes decay with time delay as more and more of the wave packet is dissociated and the shoulder becomes less prominent. The interesting aspect of the dynamics is that the GA captures the "essence" of the wave packet evolution and without specific knowledge of the system it is able to fire the second laser at appropriate moments.

Next, we shall discuss the effect of laser chirp. The distribution of the chirp values in Fig. 4(b) finds a prominent peak at a small value of about $\alpha_2 = -3.2 \times 10^{-6}$ s^{-2}. The dependence of the branching ratio on laser chirp is shown in Fig. 7(a) for $t_d = 118$ fs and $\phi = 4/15\pi$. It is seen that peak values of I^*/I are associated with chirp values close to α_2^*. Interestingly enough, a zero chirp produces the smallest value of I^*/I in the range displayed. There is also a smaller peak on the positive chirp axis, but the learning algorithm hangs in on the largest ratio. It should be noted that in a different slice along the chirp axis at another value of t_d (

≈ 1.2 ps), for which the I^*/I ratio is reasonably high as well, the behavior in Fig. 7(a) near the optimal chirp value reverses and the chirp producing the largest I^*/I is a small, but positive value. Clearly, it is evident that small chirping of the laser pulse profoundly affects the I^*/I ratio and an unchirped pulse is ineffective in enhancing I^* production.

The distribution of the 50 best phase values found by the GA [see Fig. 4(c)] suggests that I^*/I is a periodic function of the phase ϕ. To see the importance of this parameter and to corroborate our assumption, we sliced through the parameter space along the periodic phase axis. The results are shown in Fig. 7(b) and it depicts a periodic behavior of the branching ratio as a function of ϕ, implying that coherent control of I^* production is possible. However, the amplitude of the oscillation is small, indicating that the phase is not as important a parameter as the time delay or the chirp.

IV. SUMMARY AND CONCLUSIONS

The dynamical behavior of NaI photodissociation using a two-laser pump-control scheme is investigated and the branching ratio for the excited to ground state iodine atom production is calculated as a function of the time delay between the pump and control pulses. A learning algorithm is implemented to explore the laser parameter space to find optimal and experimentally realizable parameters (time delay, chirp, and phase) that would maximize the I^*/I branch-

ing ratio. Our calculations show that without having prior specific knowledge of the wave packet dynamics, the learning algorithm is able to tailor a control laser pulse to yield maximum value for the I^*/I branching ratio.

The control scheme employed here is similar to the Tannor-Rice scheme, and it uses suitable time delays between the pump and control laser pulses to control nuclear motion on the different potential curves. The calculation also revealed an interesting and experimentally important fact: the laser chirp, however small, has a significant effect on I^* production—the I^*/I branching ratio increases by more than an order of magnitude with a chirped pulse. The phase as a coherent control parameter is found to have a relatively small, but periodic effect on the I^*/I ratio, revealing that the output channel can be controlled by constructive and destructive interferences between wave packets propagating on different potential curves.

[1] W. Ketterle, Rev. Mod. Phys. **74**, 1131 (2002).

[2] M. Greiner, C. A. Regal, and Deborah S. Jin, Nature (London) **426**, 537 (2003).

[3] F. Pereira Dos Santos *et al.*, Phys. Rev. Lett. **86**, 3459 (2001).

[4] N. R. Claussen *et al.*, Phys. Rev. A **67**, 060701(R) (2003).

[5] T. Brabec and F. Krausz, Rev. Mod. Phys. **72**, 545 (2000).

[6] D. H. Sutter *et al.*, Opt. Lett. **24**, 631 (1999).

[7] N. Bloembergen, Rev. Mod. Phys. **71**, S283 (1999).

[8] M. R. Dantus, R. M. Bowman, and A. H. Zewail, Nature (London) **343**, 737 (1990).

[9] A. Mokhtari, P. Cong, J. L. Herek, and A. H. Zewail, Nature (London) **348**, 225 (1990).

[10] M. Shapiro and P. Brumer, Adv. At., Mol., Opt. Phys. **42**, 287 (2000).

[11] P. Brumer, Photonics Spectra **30**, 83 (1996).

[12] D. Tannor and S. A. Rice, J. Chem. Phys. **83**, 5013 (1985).

[13] D. Tannor, R. Kosloff, and S. A. Rice, J. Chem. Phys. **85**, 5805 (1986).

[14] R. J. Gordon and S. A. Rice, Annu. Rev. Phys. Chem. **48**, 601 (1997).

[15] T. S. Rose, M. J. Rosker, and A. H. Zewail, J. Chem. Phys. **88**, 6672 (1988).

[16] T. S. Rose, M. J. Rosker, and A. H. Zewail, J. Chem. Phys. **91**, 7415 (1989).

[17] P. Cong, A. Mokhtari, and A. H. Zewail, Chem. Phys. Lett. **172**, 109 (1990).

[18] A. H. Zewail, J. Phys. Chem. **100**, 12701 (1996).

[19] J. L. Herek, A. Materny, and A. H. Zewail, Chem. Phys. Lett. **228**, 15 (1994).

[20] M. Baba, T. Kokita, S. Kasahara, and H. Katô, J. Chem. Phys. **111**, 9574 (1999).

[21] V. Engel *et al.*, Chem. Phys. Lett. **152**, 1 (1988).

[22] V. Engel and H. Metiu, J. Chem. Phys. **90**, 6116 (1989); **91**, 1596 (1989).

[23] S. E. Choi and J. C. Light, J. Chem. Phys. **90**, 2593 (1989).

[24] Y. Sakai, E. Miyoshi, and T. Anno, Can. J. Chem. **70**, 309 (1992).

[25] J. R. Waldeck, M. Shapiro, and R. Bersohn, J. Chem. Phys. **99**, 5924 (1993).

[26] T. J. Martinez and R. D. Levine, Chem. Phys. Lett. **259**, 252 (1996).

[27] C. J. Bardeen *et al.*, J. Phys. Chem. A **101**, 3815 (1997).

[28] H. Tang and S. A. Rice, J. Phys. Chem. A **101**, 9587 (1997).

[29] G. H. Peslherbe *et al.*, J. Chem. Soc., Faraday Trans. **93**, 977 (1997).

[30] M. Grønager and N. E. Henriksen, J. Chem. Phys. **109**, 4335 (1998).

[31] P. Marquetand, A. Materny, N. E. Henriksen, and V. Engel, J. Chem. Phys. **120**, 5871 (2004).

[32] N. Balakrishnan, B. D. Esry, H. R. Sadeghpour, S. T. Cornett, and M. J. Cavagnero, Phys. Rev. A **60**, 1407 (1999); S. T. Cornett, H. R. Sadeghpour, and M. J. Cavagnero, Phys. Rev. Lett. **82**, 2488 (1999).

[33] A. B. Alekseyev *et al.*, J. Chem. Phys. **113**, 1514 (2000).

[34] T. P. Rakitzis *et al.*, Science **300**, 1936 (2003).

[35] M. D. Feit, J. Fleck, Jr., and A. Steiger, J. Comput. Phys. **47**, 412 (1982).

[36] N. Balakrishnan, C. Kalyanaraman, and N. Sathyamurthy, Phys. Rep. **280**, 79 (1997).

[37] N. Balakrishnan, A. B. Alekseyev, and R. J. Buenker, Chem. Phys. Lett. **341**, 594 (2001).

[38] D. E. Goldberg, *Genetic Algorithms in Search, Optimization, and Machine Learning* (Addison-Wesley, Reading, MA, 1989).

[39] X. Chu and Shih-I Chu, Phys. Rev. A **64**, 021403(R) (2001).

[40] J. J. Grefenstette, computer code GENESIS v. 5.0, 1990.

[41] http://cfa-www.harvard.edu/~bhadjiho/animations/